Conference on Modelling Fluid Flow (CMFF'25)
The 19th International Conference on Fluid Flow Technologies
Budapest, Hungary, August 26-August 29, 2025

NUMERICAL ANALYSIS OF SWIRLING FLOW INDUCED BY AXIAL FAN

Aleksandar Ćoćić[1], Balazs Pritz[2]

[1] Corresponding Author. University of Belgrade - Faculty of Mechanical Engineering, Chair for Fluid Mechanics. Kraljice Marije 16, 11120 Belgrade, Serbia. Email: acocic@mas.bg.ac.rs
[2] Institute for Thermal Turbomachinery (ITS), Karlsruhe Institute of Techonology (KIT), Kaiserstraße 12, D-76131 Karlsruhe, Germany. Email: pritz@kit.edu.

ABSTRACT

In this paper, swirling flow generated by axial fan at the beginning of long, horizontal pipe is studied in great detail using numerical computations. In order to have the least possible effect of mesh parameters to the accuracy of computations, great attention is dedicated to creation of high quality block-structured grid, which also includes the geometry of axial fan. Flow is then studied using two approaches: frozen-rotor with RANS models (RNG k-ε and k-ω SST). For aforementioned computation OpenFOAM® is used. Additionally, using block-structured in-house code SPARC at KIT, flow is computed using LES with MILES approach. Experimental results of mean velocity profiles and turbulent kinetic energy were used as validation tool. Obtained results give deeper insights into the dynamics of vortex structures and the process of swirl decay, where good agreement is found with experimental results.

Keywords: swirling flow, axial fan, CFD, RANS, LES.

NOMENCLATURE

$\underline{U}$	$[m/s]$	averaged (filtered) velocity vector
$\underline{U}_r$	$[m/s]$	relative averaged velocity vector in rotating frame of reference
P	$[m^2/s^2]$	averaged (filtered) kinematic pressure
$\underline{\tilde{u}}$	$[m/s]$	instantaneous velocity vector
$\tilde{p}$	$[m^2/s^2]$	instantaneous kinematic pressure
k	$[m^2/s^2]$	turbulent kinetic energy
ν	$[m^2/s^2]$	molecular viscosity
ν_t	$[m^2/s^2]$	turbulent viscosity
ω	$[1/s]$	specific rate of dissipation of turbulent kinetic energy
ε	$[m^2/s^3]$	dissipation rate of turbulent kinetic energy
$\underline{\Omega}$	$[1/s]$	angular velocity vector

1. INTRODUCTION

Swirling flows occurs frequently, both in nature and engineering. Typical examples from nature are hurricanes and tornadoes in Earth's atmosphere and whirlpools in seas and oceans. Fluid flows in turbomachinery, cyclone separators, combustion chambers and pipeline systems - to name a few, are examples from engineering. These flows can be viewed as combination of plane rotational flow and axial flow perpendicular to the plane, which causes the fluid to move in helicoidal trajectories. Essentially, in these flow fields we have large three-dimensional vortex structures and their interaction. In terms of modeling, we have velocity gradients in radial direction of axial and circumferential velocity with the same order of magnitude, streamline curvature and highly anisotropic structure of turbulence. Because of all that, swirling flows are typical example where RANS eddy-viscosity models fail to predict the flow development in correct manner. Some improvements are made by adding additional terms in model equations which takes the fluid rotation into the account, or by introducing the non-linearity in eddy-viscosity concepts. Reynolds stress transport models (RSTM) gives better predictions, but they have issues with computational stability.

2. FLOW MODELING

First, details about the geometry of the flow domain is presented. Then, the procedure about the creation of numerical mesh is explained in details. Finally, governing equations and constitutive model equations are presented.

2.1. Geometry, computational domain and numerical mesh

Photograph of experimental installation is shown in Fig. 1. It consists of axial fan mounted at the entrance of the long pipe. At the pipe entrance, before the fan, bell mouth is installed to minimize local losses and to produce smooth entrance of the air. Axial fan has seven straight blades, with angle of

26° toward the flow direction. Comprehensive measurements were performed on this experimental rig in past decades. It is designed and constructed by late prof. Miroslav Benišek. His was a pioneer in experimental investigation of swirling flow at Belgrade University - Faculty of Mechanical Engineering, [1]. After his original work, detailed research with various experimental techniques were performed at the same rig. Detailed description about the results and more can be found in review paper [2].

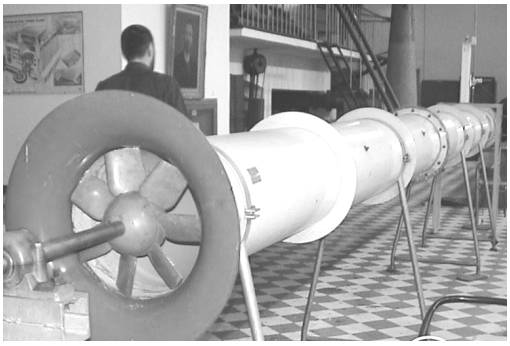

Figure 1. Photograph of experimental installation (Laboratory for Hydralic Machines, Universtity of Belgrade - Faculty of Mechanical Engineering).

The sketch of the installation, with relevant geometrical parameters is shown in Fig. 2. Their values are: $D = 400\,mm$, $D_1 = 659.6\,mm$, $\delta = 3\,mm$, $L_1 = 60\,mm$ and $L_2 = 5\,m$. It can be noted that the shaft of the fan impeller is not taken into the account. This is due to the fact that our region of interest is behind the fan.

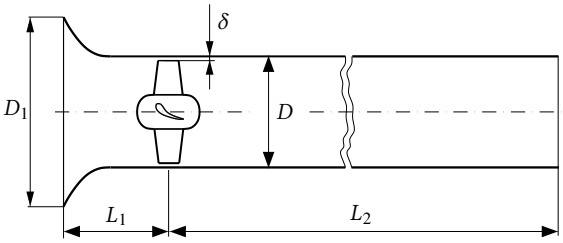

Figure 2. Sketch of experimental installation with relevant geometrical parameters.

The main goal from the start was to create numerical mesh with high quality cells, so great care is taken to create the block-structured grid, and for that purpose commercial software ICEM-CFD was used. Since it is practically impossible to create the unified block topology in whole computational domain, it is divided in three subdomains $\mathcal{D}_1$, $\mathcal{D}_2$ and $\mathcal{D}_3$. Additionally, the inlet is further extended by adding semi-spherical domain before the bell mouth in order to simulate the entrance of the air to the impeller more accurately. This is shown in Fig. 3. In flow direction, subdomain $\mathcal{D}_1$ ends up with the surface (patch) named SRI-1. This surface is geometrically the same as surface RSI-1, which is the left boundary surface of subdomain $\mathcal{D}_2$. Similar story is with right boundary surface RSI-2 and left boundary surface of subdomain $\mathcal{D}_3$, named SRI-2. Now, in these subdomains block-structured grid is created, with different topology of the blocks in each one of them.

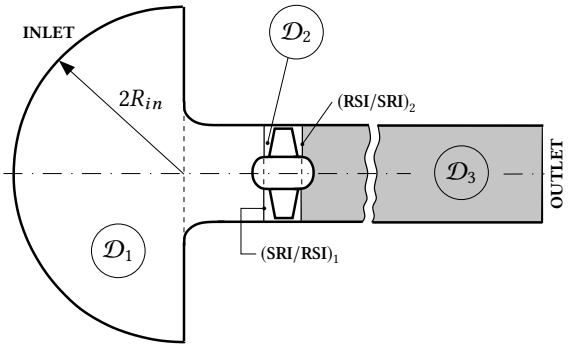

Figure 3. Computational subdomains with characteristic surfaces.

It is assured that aspect ratio between the cells in the boundary region between the domains has approximately the same size. Number of the faces of interface surfaces (SRI/RSI) is not the same, but it is assured that the difference is as small as possible, in order to reduce the error of interpolation during numerical computations. The result of that is the mesh which part around the fan impeller is shown in Fig. 4.

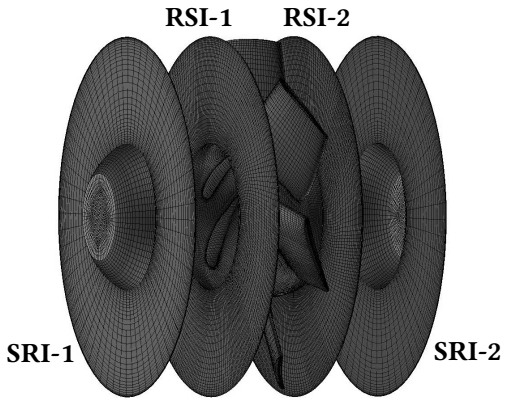

Figure 4. Part of numerical mesh with interface surfaces between the domains.

For each subdomain the minimum value of Jacobian determinant for hexahedral cells was 0.8 (mesh quality parameter in ICEM CFD; "ideal" mesh has the value of determinant 1.0 for each cell). These three meshes are exported to *.msh format, and then separately imported to OpenFOAM format using fluent3DMeshToFoam utility. Finally, they are merged together to one unique mesh with mergeMeshes utility. Cell zones in domains $\mathcal{D}_1$ and $\mathcal{D}_3$ are named STATOR-1 and STATOR-2, respectively. Cell zone in domain $\mathcal{D}_2$ is named ROTOR, and the physical rotation of the fan is treated in two different ways, which will be explained in details in following section. The results presented here are obtained on the mesh with 8265989 cells. Grid sensitivity study is performed previously and presented in [3].

2.2. Governing equations

Experiments showed that mean velocities in the pipe are around $10\,m/s$, so it is assumed that the flow is incompressible (density ρ = const). The starting point is the Navier-Stokes equations

$$\begin{aligned} &\nabla \cdot \underline{\tilde{u}} = 0 \\ &\frac{\partial \underline{\tilde{u}}}{\partial t} + \nabla \cdot \left(\underline{\tilde{u}}\, \underline{\tilde{u}} \right) = \nabla \tilde{p} + \nu \nabla^2 \underline{\tilde{u}} \end{aligned} \tag{1}$$

Because of high range of time scales and spatial vortex sizes in turbulent flows, direct numerical solution of system (1) is practically not possible for most cases. Navier-Stokes equations need additional treatment in order to reduce the range of scales. In that sense, there are two main approaches:

- time averaging, where we get the RANS equations; or ensemble averaging where we get unsteady RANS or URANS equations
- spatial filtering, where we get the filtered Navier-Stokes equations, which are the starting point for LES.

In both cases, we are splitting pressure and velocity into two parts - averaged (filtered) U_i and fluctuating remaining part u_i

$$\tilde{u}_i = U_i + u_i, \qquad \tilde{p} = P + p$$

Inserting this into the equation (1) we end up with the same type of the equations. They are

$$\begin{aligned} &\nabla \cdot \underline{U} = 0 \\ &\frac{\partial \underline{U}}{\partial t} + \nabla \cdot \left(\underline{U}\, \underline{U} \right) = \nabla P + \nu \nabla^2 \underline{U} - \nabla \cdot \underline{\underline{T}}_{\text{tur}} \end{aligned} \tag{2}$$

where $\underline{U}$ and P are ensemble (Reynolds) averaged velocity and pressure in URANS (RANS) approach, while in LES approach it is filtered velocity and filtered pressure. Symbol T_{tur} represent the second order tensor which originates from averaging or filtering procedure of the original nonlinear convective term in Navier-Stokes equations. In RANS modeling turbulence tensor T_{tur} is called Reynolds stress tensor and it is modeled by introducing turbulent viscosity ν_t, which was known as Boussinesq approximation

$$\underline{\underline{T}}_{\text{tur}} = \nu_{\text{t}} \left(\nabla \underline{U} + \nabla \underline{U}^T \right) + \frac{2}{3} k\, \underline{\underline{I}}$$

where k is time averaged turbulent kinetic energy. Turbulent viscosity is determined from auxiliary model equations. Here we'll compare the results obtained with RNG k-ε and k-ω SST models, [4] and [5]. Similar approach is in LES, where we are introducing sub-grid scale viscosity ν_{sgs} for modeling residual stresses T_{tur}.

2.2.1. Momentum equation in rotating frame of reference

Equations (2) can be further simplified using so called "frozen-rotor" approach. Here we're assuming that the turbulence is statistically steady, we're using RANS. Rotation of the fan is taken into the account in the following way. In any fluid domain which rotates with constant angular velocity $\underline{\Omega}$ we can represent absolute velocity vector via two components, relative and rotational

$$\underline{U} = \underline{U}_r + \underline{\Omega} \times \underline{r}$$

Inserting this into the RANS equations, we'll get the equation with two additional terms: centrifugal and Coriolis force per unit mass, while the velocity vector will be $\underline{U}_r$. That is, we get RANS equation in rotating frame of reference. Since we have also the other parts of domain where we don't have physical rotation of the fluid, it is convenient to use the same convective velocity throughout the domain, which is $\underline{U}$, velocity absolute frame of reference. For that purpose, convective term with relative velocities + Coriolis force + centrifugal force, can be written as

$$\nabla \cdot (\underline{U}_r\, \underline{U}) + \underline{\Omega} \times \underline{U}$$

and system of equations (2) becomes

$$\begin{aligned} &\nabla \cdot \underline{U} = 0 \\ &\nabla \cdot (\underline{U}_r\, \underline{U}) = \nabla P + \nu \nabla^2 \underline{U} - \underline{\Omega} \times \underline{U} - \nabla \cdot \underline{\underline{T}}_{\text{tur}} \end{aligned} \tag{3}$$

Finally, in numerical procedure the convective term is split into two parts

$$\nabla \cdot (\underline{U}_r\, \underline{U}) = \nabla \cdot (\underline{U}\, \underline{U}) - \nabla \cdot [(\underline{\Omega} \times \underline{r})\, \underline{U}]$$

Now all the terms in Eq. (3) are written with velocity vector $\underline{U}$ in absolute frame of reference. Convection flux have additional correction term which takes into the account the rotation. Prior to computation, the position of rotational axis in absolute frame of reference needs to be specified, together with the magnitude of angular velocity $\underline{\Omega}$.

2.3. Simulation set-up

In this section detailed description of simulation set up concerning boundary conditions, discretization schemes and iterative solvers used for solution of system of linear equations is given. This is mostly related to OpenFOAM® . Boundary conditions for SPARC code are very similar, and the differences will be mention in later section, where results are presented. For all computations angular velocity of $\Omega = 104.72\,rad/s$ is set, like it was in experiment.

2.3.1. Boundary conditions

At the INLET boundary, Fig. 3, value of total pressure is specified, while at OUTLET boundary fixed value of pressure is specified. These values are assumed to be the same, equal to zero. For velocity, boundary condition called pressureInletVelocity is prescribed. The inflow velocity is obtained during the computation from the flux with a direction normal to the INLET boundary. For turbulence quantities, values based on estimated length and time scales are defined at the INLET, while like for the velocity, zero gradient is applied at the OUTLET boundary. With this setup flow through the domain is estab-

lished due to the fan rotation, which corresponds to the experimental set up. From the Figs. 3 and Figs. 4, in both STATOR cell zones, parts of the hub are located. Constant, nonuniform value of velocity is prescribed, calculated from angular velocity of the fan and the radial distance from rotational axis. At all patches of type wall, zero gradient for pressure is prescribed, while for turbulence quantities wall functions were used. Two version of OpenFOAM were used for computations:

1. ESI-OpenCFD version OpenFOAM® 2306, [6], named OFv2306 in further text, and
2. foam-extend version 4.1, a fork of the OpenFOAM® driven by the community [7], named FE41 in further text

While aforementioned boundary conditions are the same in both version, different boundary conditions are used at the non-conformal interfaces SRI/RSI.

In early stages, when it was announced in 2012, only extended version had the capabilities to compute turbomachinery problems. One on the main issues which needed to be solved is how to handle non-conformal interfaces. At that time the generalized grid interface (GGI) was presented and implemented in the original OpenFOAM code [8]. At the interface, the level of communication between the cells is established first, depending of the relative face overlap. The effect of facets is interpreted by a facet-area-based interpolation scheme across the interface. Interpolation stencil is established by geometrical consideration and weighting factors are calculated as area ratio of the facet and the complete face [8]. Additionally, mixing plane boundary condition is also introduced in [8] where the averaging of the flow variables in circumferential direction is performed at second interface in the pair (SRI-2) at each time step, while preserving the flux through the face. Using that approach, we have axisymmetric conditions at the SRI-2, at the pipe inlet. GGI and mixing plane boundary conditions are further improved in terms of stability, and they're available in FE41.

In OFv2306 boundary condition named cyclicAMI (AMI as abbreviation for Arbitrary Mesh Interface) uses the same principle as GGI, and it's based on the original code of GGI. Additional weighting factors are introduced in order to establish more robust interpolation at the interfaces.

2.3.2. Discretization and iterative solvers

Second order linear upwind scheme is used for discretization of convective terms for velocity and turbulence quantities. Initial computations started with purely upwind schemes on all variables, and later during computations, when converged solution is established, schemes are switched to linear upwind. Computations were performed in parallel mode, on 32 Intel® Xeon® Silver 4108 CPUs.

Concerning iterative solver for pressure, it was found that in FE41 preconditioned conjugated gradient (PCG) solver for pressure was faster and more stable in comparison to generic algebraic multigrid (GAMG). In some cases, computations with GAMG were extremely slow. It is assumed that this problem is related to distribution of computation between the nodes, but it wasn't investigated in greater details, since PCG showed stable and accurate. In OFv2306 GAMG solver showed robust and smooth. Concerning the computational time between two version, we didn't perform real tests. The computations in "frozen-rotor" approach are performed in following way:

(1) OFv2306, RNG k-ε, with constant, near zero values inside the domain for all physical quantities
(2) OFv2306, k-ω SST model, using the converged solution from (1) as the initial values; initial values of omega is calculated from k and ε using turbulenceFields function object
(3) FE41, RNG k-ε, using the converged solution (1) as the initial values
(4) FE41, k-ω SST mode, using the converged solution (2) as the initial values.

Of course, for (3) and (4) we needed to tweak few files, to adopt it to the requested syntax. Additionally, for both (3) and (4) both GGI and mixing plane at the interface RSI-2/SRI-2 are used.

3. RESULTS AND DISCUSSION

In [9] comprehensive measurements were performed at experimental rig shown in Fig. 1. Those experimental results are used as the validation tool.

3.1. Results of "frozen-rotor" approach

First, we analyze the global parameters like volume flow rate through the domain. These results are shown in Table 1, together with percentage difference between the values. In calculation of the

Table 1. Volume flow rate values (in m^3/s).

	FE41	**OFv2306**	**Difference**
RNG k-ϵ	0.61753	0.61005	1.23%
k-ω SST	0.63145	0.62381	1.69%
Difference	2.23 %	2.23 %	

percentage difference, we used the arithmetic mean in denominator, and the absolute value of difference in numerator. Values in last columns corresponds to the difference between versions, with the same turbulence model in both version. Difference given in last row is due to the choice of turbulence model, within the same version. It is notable that k-ω SST predicts larger flow rate in comparison to RNG k-ε model, and that percentage is almost the same in both version. There is also a slight difference for both turbulence models between the versions, and that difference is a bit more pronounced in case of k-ω SST model. In terms of stability and robustness of computations, version OFv2306 showed great advantages. Convergence is monitored in several ways.

First, by values of residuals during iterative procedure. Second, by monitoring the flow rate, and lastly monitoring the values of velocity and pressure in several points inside the domain. In both versions, RNG k-ε model lead to steady-state solution, while in case of k-ω SST we have pseudo-steady solution. This can be seen in Fig. 5.

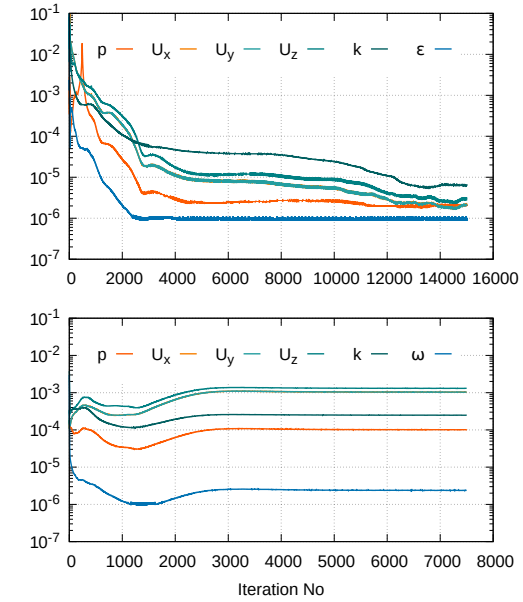

Figure 5. OFv2306. Residuals of physical quantities during computations with RNG k-ε (top) k-ω SST model (bottom).

It is worth mentioning again that initial values of physical quantities inside the domain for computations with k-ω SST are converged solution obtained with RNG k-ε model. After initial decrease in residual values for all physical quantities, they start to increase, and after 3000 iteration they remain constant in further computations. Such changes of residuals indicates the unsteady behaviour of solution.

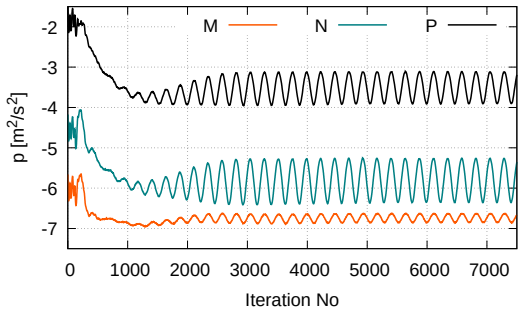

Figure 6. OFv2306, k-ω SST. Variation of pressure in several points in cross-section $z = 0.1\,m$. Coordinates (x, y) of the points are: M(-0.05, 0); N(-0.1, 0) and P(-0.175, 0).

This is evident from the diagram shown in Fig. 6, where oscillations of pressure in different points during iterations are shown. It can be seen that oscillation period is the same for all points, while the amplitude is different. Concerning oscillation period we have roughly four periods in 1000 outer iterations. Of course, we can not talk about accurate unsteady dynamics in this case, but it is interesting to see how global flow field is changing during iterations. The changes of velocity and pressure during iterations are shown in Fig. 7.

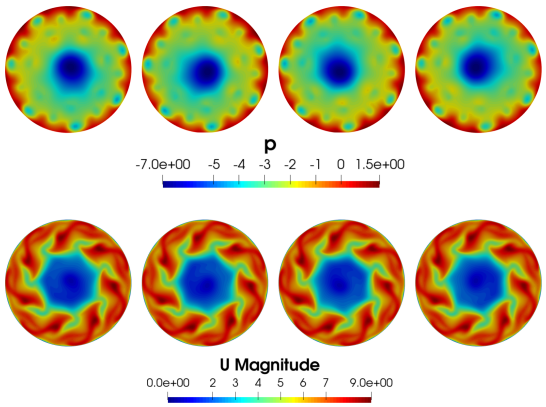

Figure 7. OFv2306, k-ω SST. Contours of pressure (in m^2/s^2) and velocity magnitude (in m/s) in cross-section $z = 0.25\,m$, in outer iterations 4000, 5000, 6000 and 7000. Back view, from pipe outlet.

We can see that main changes are located in the core region of the pipe. Based on contours of low pressure region, these changes of pressure resemble to unsteady vortex rope behind the fan. This vortex rope can be better visualized using Q criterion. Three-dimensional contour of constant Q is shown in Fig. 8.

Figure 8. OFv2306, k-ω SST model. Vortex structures identified as contour of $Q = 1500\,s^{-1}$. Outer iteration number 5000.

Besides coherent vortex structure in the central region of the pipe, e.g. vortex core, we also have additional seven larger structures which originates from the tips of the fan blades. These contours passes through regions of low pressure near the pipe wall shown in Fig. 7. But, contrary to movement of vortex rope in the central region of the pipe, those vortex structures remain still during iterations. This is expected, since in the position of the fan is frozen, and this structures are located near the pipe wall.

Due to fact that we have oscillatory behaviour

during iterations, we can get from this quasi steady to steady solution in following way. Rough estimate is that 4000 iterations is needed for the rope to make one quasi-revolution. In that sense, we can start do compute moving averages (UMean and pMean) from 4000 to 8000 iteration in order to get iteration averaged values of pressure and velocity in each point of computational domain. Using this procedure, we can get the steady state solution. This is shown in Fig. 9 where contours of velocity magnitude are shown, for both turbulence models. In case of RNG k-ε model it is converged velocity, while in case of k-ε SST model it is the iteration averaged velocity.

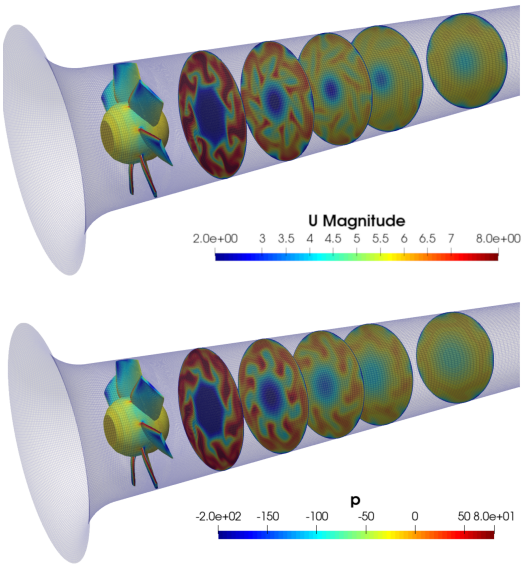

Figure 9. OFv2306. Contours of velocity magnitude (in m/s) in several cross-sections behind the fan: z = 0.25, 0.5, 0.75, 1 and 1.5 m. Contours of kinematic pressure (in m^2/s^2) are shown at fan blades and hub. Top: RNG k-ε, bottom: k-ω SST model.

From Fig. 9 we can clearly see the difference in the results between two models. The effect of the position of fan impeller is more pronounced in case of k-ω SST model. It is evident that the flow is not purely axisymmetric in cross-section close to the fan impeller, it is rather quasi-periodic with $360°/7$ (number of fan blades is seven). Due to many practical reasons, velocity components in OpenFOAM® are stored and calculated in Cartesian coordinates. Based on those results, velocity components in polar coordinates are calculated. For swirling flow, radial distribution of circumferential component can be used to characterize the type of the flow. This distribution is shown in Fig. 10, for both models, in cross-section $z = 1\,m$ of the pipe. For k-ω SST model we used mean velocity vector UMean. From the Fig. 10 it evident that we have so called solid-body rotation, where circumferential velocity reaches maximum values close to the pipe wall, and of course has its minimum in the axis region. Position of

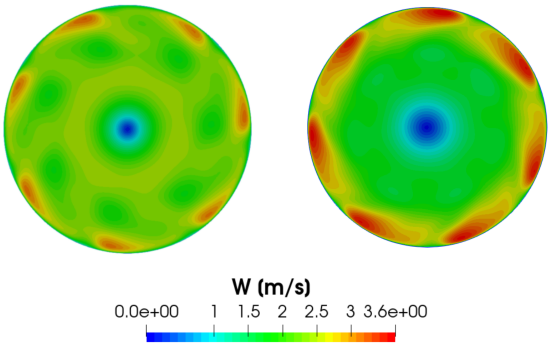

Figure 10. OFv2306. Contours of circumferential velocity W in cross-section $z = 1\,m$. Left: RNG k-ε, right: k-ω SST model.

these regions where circumferential velocity reaches its maximum are directly related to the position of the fan blades, and the profile is not axisymmetric. We can perform circumferential averaging as a part of post-processing in any chosen cross-section, but this is a bit tedious work. For that purpose we used mixing plane at interface, a boundary condition available in version FE41.

3.1.1. Comparison to experimental results

In LDA measurements it was assumed that flow is axisymmetric, and measurements are performed in vertical plane, as shown in Fig. 11.

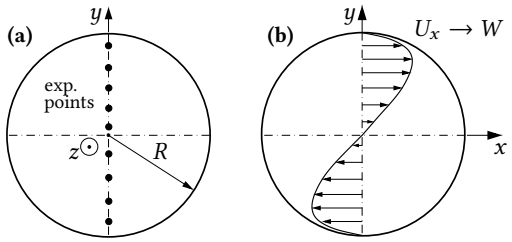

Figure 11. (a) Position of measuring points in cross-section of the pipe. (b) Mean velocity component in direction of x axis corresponds to circumferential component of velocity in polar coordinates.

Additionally, it is assumed that radial velocity component is much smaller in comparison to axial and circumferential, and it wasn't measured. This is usual and accurate approximation for this type of swirling flow. In order to do comparison to the experimental results, i.e. to compare the mean velocity components U_x and U_z, numerical results obtained with mixing plane interface in FE41 are chosen, since they produce axisymmetric flow in the pipe. This is shown in Fig. 12, where symmetry of flow variables in measuring cross-section in circumferential direction is evident. That symmetry is also pronounced in all other cross-sections of the pipe. In that sense, there is no need to calculate velocity components in polar coordinates as a part of post-processing procedure. Instead, velocity component normal to the

sampling line in cross-section will correspond to the circumferential component.

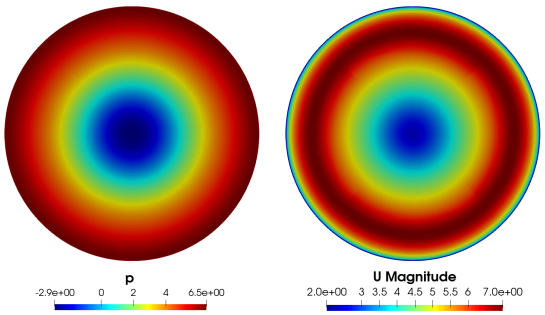

Figure 12. FE41. Contours: kinematic pressure (m^2/s^2), left, and velocity magnitude (right). RNG k-ε turbulence model, measuring section $z = 1\,m$. Mixing plane at the interface pair RSI-2/SRI-2.

Comparison of velocity distribution along vertical axis to experimental results is shown in Fig. 13. Very good agreement is found, for both turbulence models. Decrease in axial velocity in core region is captured in correct manner, and also the type of circumferential velocity profile. There is slight underestimation of the slope of circumferential velocity profile around the axis, which results in underestimation in whole cross-section, except the wall region.

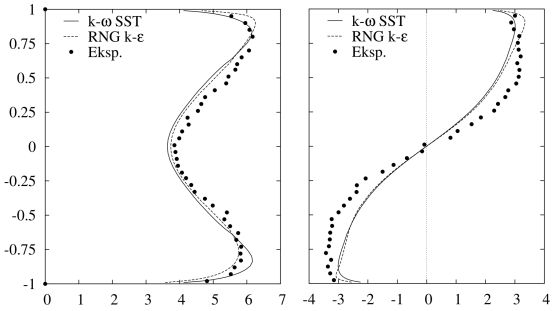

Figure 13. FE41. Comparison of axial and circumferential velocity profiles (see Fig. 11), measuring section $z = 1\,m$. Mixing plane at the interface pair $(\mathrm{RSI/SRI})_2$.

There are numerous experimental points. The reason for that is to check if the assumption of axisymmetry is fulfilled. We can see that there are slight deviation between the values in points which are symmetric around the axis. However, maximum of this deviation is not larger than 2% between the points. Also, in region around the pipe axis, unsteadiness is highly pronounced, specially in circumferential direction. More details about the problems with measurements in this region can be found in [9]. In that region we can also have back flow, or even axial velocity equal to zero. This decrease in axial velocity in core region are directly related to the existence of rotational, i.e. circumferential velocity component.

3.2. Results of the SPARC code

Quasi-steady behaviour shown in Fig. 6 and Fig. 7 clearly shows that this kind flow is unsteady in nature, even on larger scales. This behaviour in results was not found with RNG k-ε model, where we get steady solution. Of course, the most accurate solution with both turbulence models will be with mesh rotation. But, for the purpose of presenting the results in this paper, on this mesh with available computational power, it seems like impossible task. So we turned to the SPARC code. SPARC is in-house block-structured CFD code, written in FORTRAN and developed at KIT Institute of fluid machinery. Foundation of the code are compressible Navier-Stokes equations. Modeling of sub-grid scales in LES are based on MILES algorithm. In contrast to OpenFOAM® , where computations are performed on unstructured mesh by definition, computations in SPARC are performed on mesh defined as multi-block mesh. The topology of the blocks in mesh generation process is important parameter for computations. It turned out that mesh which one part shown in Fig. 4 was very good in that sense, and the simulations ran smooth. For temporal discretization second order dual time stepping is used, with time step in range $\Delta t = 10^{-5}\,s$. For more stable computations, constant flow rate is prescribed at the INLET. At the interfaces SPARC uses sliding mesh approach. After more ten flow through times, values of physical quantities are averaged in time, in order to validate the computation with comparison to the experimental results. Very good agreement is found in terms of axial and circumferential velocities, as shown in Fig. 14. In contrary to Fig. 13 circumferential averaging is performed for both experimental and numerical results.

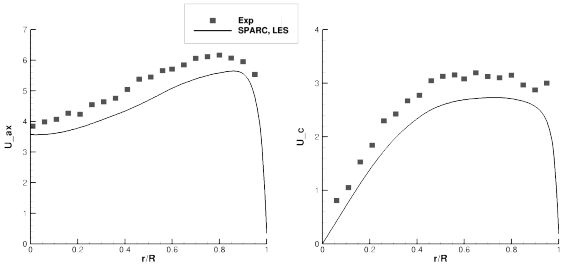

Figure 14. SPARC. Profiles of axial and circumferential velocity in cross-section $z = 1\,m$.

Since in experiments LDA method is used, with sampling rate of $2\,kHz$, it is possible to calculate the root mean square (RMS) of signals that corresponds to axial and circumferential velocity, and compare it with results from SPARC. In Fig. 15 RMS values of axial and circumferential velocity are shown. In contrast to Fig. 13, experimental values are taken as arithmetic mean value of two symmetric points in respect to axis (dependence of radial coordinate). There are two peak values in RMS of axial velocity, which are also predicted numerically. One is located

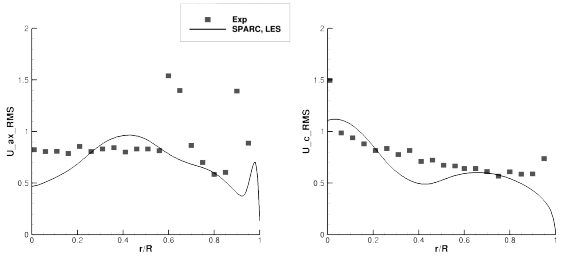

Figure 15. SPARC. Turbulence intensities, i.e. root mean square of axial (left) and circumferential velocity (right) in cross-section $z = 1\ m$.

in the wall region where large velocity gradients produces turbulent kinetic energy, and other at the end of vortex core region where large velocity gradients are also present. Both of these maximums are largely under-predicted in comparison to experimental results. On the other hand, there is good agreement in terms of RMS of circumferential velocity. Figure 16 shows unsteady vortex rope in the region near the pipe axis, in one instant in time. Unsteady behaviour of vortex rope are captured in physically expected manner.

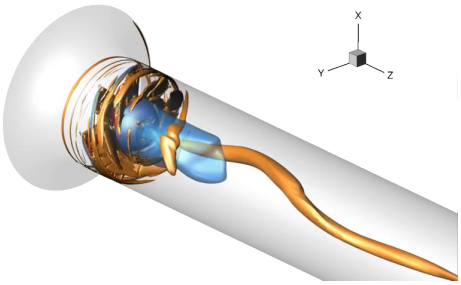

Figure 16. SPARC. Vortex rope identified by contour of constant $Q = 1000\,s^{-1}$ (orange) and contour of zero velocity (blue) in one instants of time.

Computations in SPARC were performed in parallel mode, using MPI on HP XC3000 with 120 CPUs in Scientific Computer Center of KIT. Some issues encountered during computations are given in great detail in [10]. Our opinion is that this behaviour can be reduced with dedicated non-reflecting boundary condition, which will be implemented in the code.

4. CONCLUSION

Numerical analysis of swirling flow straight circular pipe is presented in this paper. Swirl is generated by axial fan, mounted at the pipe inlet. Complete geometry is modeled, while the rotation of the fan is taken into the account in two ways: using frozen-rotor approach and using sliding mesh, with two different CFD codes: OpenFOAM® for first approach and SPARC for the second. Two different version of OpenFOAM® are tested, and it was found that there are slight differences in the results between the versions. Both codes give the results which are in good agreement with experimental results. Future research is dedicated to URANS and hybrid LES/RANS computations with rotating mesh in OpenFOAM® and improvement of LES computations in SPARC.

ACKNOWLEDGMENT

This work has been supported by the Ministry of Education, Science and Technological Development, Republic of Serbia through project 451-03-137/2025-03/20010. First author also wants the express gratitude to the students of University of Belgrade for inspiration and motivation they are giving since the beginning of December 2024.

REFERENCES

[1] Benišek, M., 1979, “Investigation of Swirling Flow in Pipe (in Serbian)”, Ph.D. thesis, University of Belgrade - Faculty of Mechanical Engineering.

[2] Benišek, M., Lečić, M., Čantrak, Dj., and Ilić, D., 2017, “The School of the Turbulent Swirling Flow at the Faculty of Mechanical Engineering University of Belgrade”, *Thermal Science*, Vol. 21, Issue suppl. 3, pp. 899–911.

[3] Ćoćić, A., Ratter, H., Lečić, M. and Gabi, 2014, M. “Numerical Investigations of Flows in Axial and Radial Fans Using OpenFOAM”, 9th International OpenFOAM Workshop - Zagreb, Croatia, June 23-26th

[4] Yakhot, V., Orszag, S., Thangam, S., Gatski, T., and Speziale, C., 1992, “Development of Turbulence Models for Shear Flows by a Double Expansion Technique”, *Physics of Fluids*, Vol. 4, No. 7.

[5] Menter, F., Kuntz, M., and Langtry, R., 2003, “Ten Years of Industrial Experience with the SST Turbulence Model”, *Heat and Mass Transfer*, Vol. 4.

[6] https://www.openfoam.com

[7] https://sourceforge.net/projects/foam-extend

[8] Jasak, H., and Beaudoin, M., 2011, “OpenFOAM Turbo Tools: From General Purpose CFD to Turbomachinery Simulations”, *Proceedings of the ASME-JSME-KSME 2011 Joint Fluids Engineering Conference*, Hamamatsu, Shizuoka, Japan, pp. 1–12.

[9] Čantrak, Dj., 2012, “Analysis of Vortex Core and Turbulence Structure in Circular Pipe With PIV, LDA and HWA methods”, Ph.D. thesis, University of Belgrade - Faculty of Mechanical Engineering.

[10] Pritz, B. and Gabi, M. 2017, “On the Resonant Behaviour of Compressible Flow Simulations”, *Proceedings of the 13th International Symposium on Experimental Computational Aerothermodynamics of Internal Flows*, 7-11 May, Okinawa, Japan